

基于Maxwell的爬壁机器人磁轮磁吸力特性分析

张文强¹ 宾光富² 徐光平¹ 杨文明¹

(1. 北京中安吉泰科技有限公司, 北京 100085)

(2. 湖南科技大学 机械设备健康维护湖南省重点实验室, 湘潭 411201)

摘要:【目的】针对传统磁瓦式磁轮在锅炉爬壁机器人应用中存在的磁场分布不明确、经验公式安全系数冗余、磁铁利用率低及磁轮过重等核心问题,旨在找出磁轮相同体积与质量约束下,N-S交替排布中磁吸力更优的磁瓦排布方案,并明确磁轮压3根与压2根锅炉水冷壁管时的磁场分布差异及磁吸力大小。【方法】以火电锅炉水冷壁检测机器人为例,建立了4种外形尺寸相同但磁铁排布方式不同的磁轮模型;运用Maxwell软件,对4种不同结构形式磁轮在距离火电厂锅炉水冷壁2 mm时的磁吸力进行了仿真分析。【结果】结果表明,磁轮磁瓦拼接处吸附比磁瓦中间处吸附时的磁吸力大5%~20%;在磁瓦中间处吸附时,无论磁轮压3根壁管还是压2根壁管,4块磁瓦排布方式的磁轮磁吸力均最大;磁轮压3根水冷壁管比压2根水冷壁管的磁吸力大10%~20%。

关键词: 爬壁机器人; 磁轮; 永磁吸附; 磁吸力; 轮式机器人

中图分类号: TH122 **DOI:** 10.16578/j.issn.1004.2539.2026.01.007

0 引言

目前,爬壁机器人作为大型储罐、建筑幕墙、大型船舶、风电塔筒、火电锅炉等构件检测和作业的主要设备,可替代人工完成一些危险性高的作业任务。根据不同吸附方式,爬壁机器人主要分为负压式、永磁吸附式、推力吸附式^[1]。永磁吸附式爬壁机器人主要有磁轮式、履带式两种结构形式^[2]。磁轮式爬壁机器人相比履带式具有运动速度快、转向灵活等特点;同时,它因接触面积小,存在磁吸力相对较弱、越障稳定性低等问题。磁轮式爬壁机器人的磁轮是向机器人提供磁吸力的主要来源,相同质量的磁铁如何排布才能提供较大磁吸力,成为磁轮结构设计的重要因素。目前,国内外对爬壁机器人吸附单元均做了一些研究。袁夫彩等^[3]通过在两块永磁体之间增加隔磁材料的方式来增大机器人履带上吸附单元的磁吸力。赵智浩等^[4]采用正交试验设计和响应面近似模型方法,得到磁吸附单元各参数与磁吸力关系的表达式,确定优化设计模型,提高了吸附单元的吸附效率。塔月月^[5]通过对轮式机器人磁性轮和磁性吸盘模型进行仿真分析,得到磁轮宽、轮厚、宽厚比、气隙等参数对磁性轮磁吸力的影响曲线,最终确定出最佳的磁性轮和磁性吸盘的尺寸与结构。陈勇等^[6]提出一种新型H形变磁力吸附单元

机构,并采用有限元分析法对新型磁吸附单元的磁场进行分析和优化,得出新结构具有利用率高、最大最小磁吸力比值大、自身质量轻的特点。孙天圣等^[7]设计了一种基于海尔贝克阵列的新型弧形永磁吸附模块,通过增加轭铁来引导磁感线,增强了吸附单元的吸附能力。冯玉勇等^[8]设计了一种4对履带爬壁机器人,对吸附单元磁性特征进行仿真分析,得出单元磁块的磁力随宽度和长度成正比例增长的结论;高度在20 mm以下时成正比例变化,超过20 mm后变化平缓。杨怀林等^[9]对海尔贝克阵列永磁体进行研究,仿真分析履带结构永磁体磁吸力与工作间隙的关系,研发了一款吸附稳定、越障性能优越的爬壁吸附系统。张栋等^[10]设计了一种壁面自适应悬摆式磁吸附机构,采用连续非线性规划算法对悬摆式磁吸附机构的结构参数进行优化,优化后磁吸附机构的磁吸力增大了25.52%。李浩男等^[11]根据机器人在管道上稳定吸附的力平衡条件,通过Maxwell仿真软件建立永磁轮的磁力分析模型,设计确定了永磁轮尺寸。但是,目前还未见针对磁瓦式爬壁机器人磁轮采用何种方式的磁瓦排布才能获得高磁铁利用率的研究。因此,本文建立了4种外形和尺寸相同、磁铁排布方式不同的磁轮模型,运用Maxwell软件进行仿真;对4种不同排布方式的磁轮在到水冷壁管相

收稿日期: 2025-05-24

作者简介: 张文强,男,1987年生,山东菏泽人,硕士;主要研究方向为机器人机械结构设计;564379558@qq.com。

引用格式: 张文强,宾光富,徐光平,等.基于Maxwell的爬壁机器人磁轮磁吸力特性分析[J].机械传动,2026,50(1):50-55.

ZHANG Wenqiang, BIN Guangfu, XU Guangping, et al. Analysis of magnetic attraction force characteristics of wall-climbing robot magnetic wheels based on Maxwell[J]. Journal of Mechanical Transmission, 2026, 50(1): 50-55.



免费获取

同距离时对应位置的磁吸力进行分析, 得出最优的磁铁排布方式, 为后期爬壁机器人磁轮结构设计提供参考。

1 磁轮模型建立

爬壁机器人磁轮在实际应用过程中, 为避免磁铁直接与水冷壁管接触对水冷壁造成损伤, 一般通过在磁轮外包胶等方式解决。利用SolidWorks软件建立了不同磁铁排布方式的磁轮模型。由于包胶不具有隔磁作用, 因此, 设置磁轮与水冷壁管的距离为2 mm来模拟磁轮外包胶厚度。所有磁瓦在轮毂上均采用N-S交替方式排布, 如图1所示。

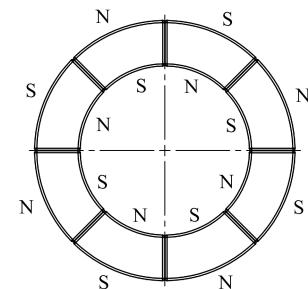


图1 磁铁排布截面图

Fig. 1 Cross-sectional diagram of the magnet arrangement

由于磁轮磁瓦采用N-S交替排布方式, 磁铁拼接处的磁力线相对较密, 单块磁瓦中间处磁力线相对较弱。以磁铁拼接处吸附均压3根水冷壁管为例, 建立2、4、8、16块磁瓦磁轮模型。4种磁轮模型磁铁的总体积和质量相等, 分析4种磁轮对水冷壁管所产生的磁吸力大小。模型分别如图2~图5所示。

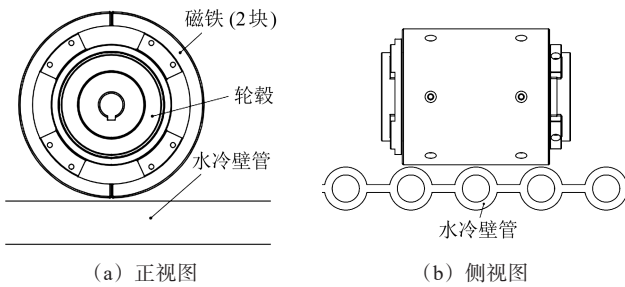


图2 2块磁瓦磁轮模型

Fig. 2 Model of the magnetic wheel with 2 magnetic tiles

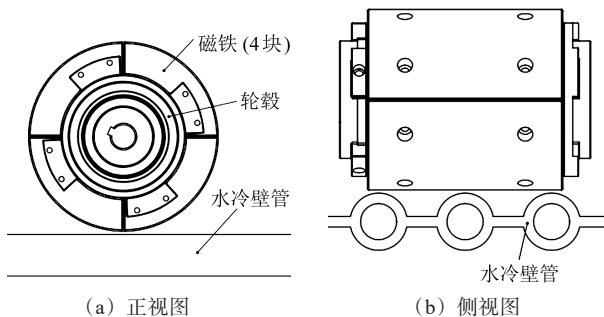


图3 4块磁瓦磁轮模型

Fig. 3 Model of the magnetic wheel with 4 magnetic tiles

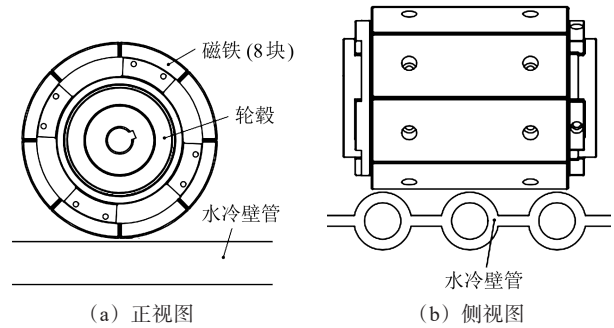


图4 8块磁瓦磁轮模型

Fig. 4 Model of the magnetic wheel with 8 magnetic tiles

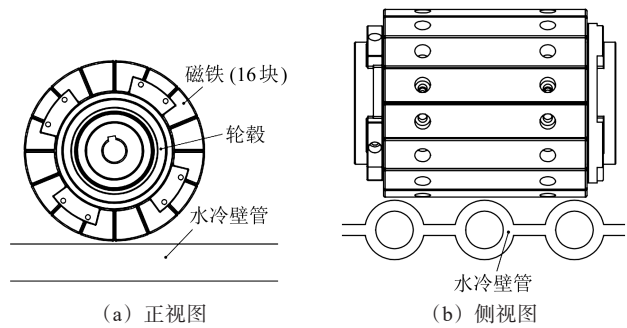


图5 16块磁瓦磁轮模型

Fig. 5 Model of the magnetic wheel with 16 magnetic tiles

分别转动每种模型中磁轮单块磁瓦中间处, 对吸附水冷壁进行仿真, 得出4种不同排布方式的磁轮单块磁瓦中间处吸附所产生的磁吸力大小。

另外, 为对比分析磁轮压2根与压3根壁管磁轮磁场分布及磁轮磁吸力的大小, 以磁轮压2根管单块磁瓦中间处吸附时为例, 分别建立2、4、8、16块磁瓦磁轮模型, 分析4种磁轮压2根水冷壁管单块磁瓦中间处吸附时的磁场分布情况及磁轮磁吸力大小。模型分别如图6~图9所示。

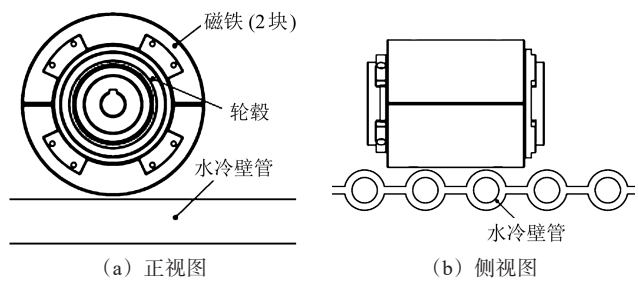


图6 磁轮压2根管时的2块磁瓦磁轮模型

Fig. 6 Model of the magnetic wheel with 2 magnetic tiles pressing against two tubes

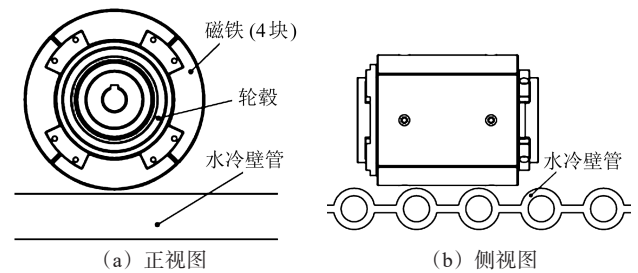
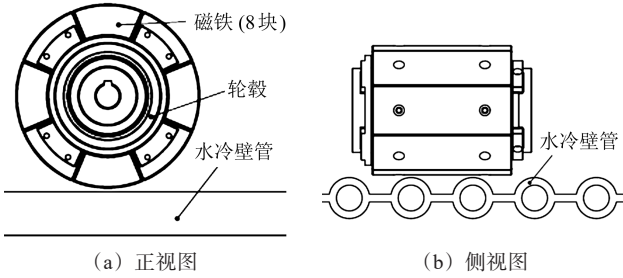


图7 磁轮压2根管时的4块磁瓦磁轮模型

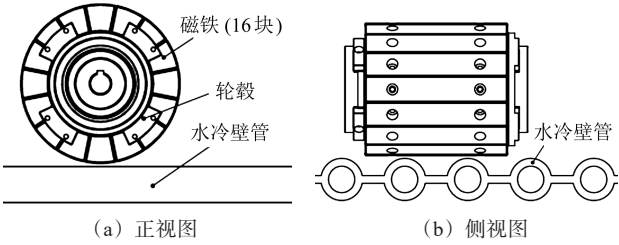
Fig. 7 Model of the magnetic wheel with 4 magnetic tiles pressing against two tubes



(a) 正视图 (b) 侧视图

图8 磁轮压2根管时的8块磁瓦磁轮模型

Fig. 8 Model of the magnetic wheel with 8 magnetic tiles pressing against two tubes



(a) 正视图 (b) 侧视图

图9 磁轮压2根管时的16块磁瓦磁轮模型

Fig. 9 Model of the magnetic wheel with 16 magnetic tiles pressing against two tubes

2 磁轮磁吸力仿真分析

2.1 磁铁拼接处吸附仿真分析

将建立好的4种不同排布方式的磁铁拼接处吸附的磁轮模型导入Maxwell软件。对磁铁、轮毂及水冷壁模型分别设置为N50钕铁硼、7075铝合金、碳钢材质；N50钕铁硼材质的剩磁 B_r 为1.43 T，矫顽力为1 051 kA/m；采用直角坐标系设置每一块磁铁的充磁方向；铝合金和碳钢采用软件自带的材料默认参数。设置仿真计算区域为50 cm×50 cm×50 cm，覆盖包含整个仿真模型。建好的仿真区域模型如图10所示。

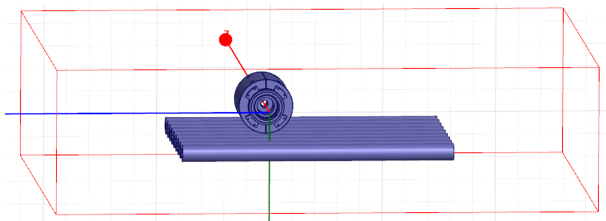


图10 仿真区域模型

Fig. 10 Model of the simulation area

磁轮由多个磁铁组成，每块磁铁产生的磁吸力不同，直接求解磁轮产生的磁吸力不方便；而磁轮所产生的磁吸力为水冷壁管受力，通过分析水冷壁管受力大小，可得出不同排布方式的磁轮磁吸力大小。以2、4、8、16块磁瓦磁轮磁铁拼接处距离水冷壁2 mm工况为例，分析了不同排布方式磁轮磁吸力大小。图11~图14为不同磁轮磁力线分布及磁感应强度分布云图。

由图11~图14可知，在距水冷壁管2 mm处、磁铁拼接处吸附时，4块磁瓦排布磁轮的磁感应强度较

其他3种排布方式大。磁铁拼接处吸附时4种排布方式磁轮距水冷壁管2 mm时产生的磁吸力如表1所示。

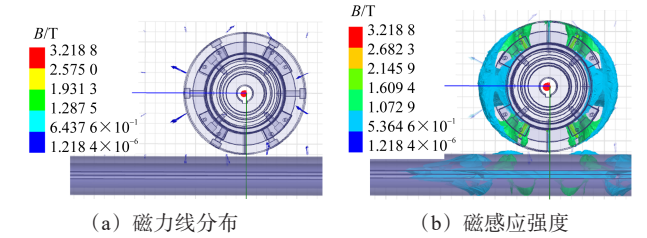


图11 磁瓦拼接处吸附时2块磁瓦磁轮的磁力线分布及磁感应强度云图

Fig. 11 Magnetic field lines and magnetic induction intensity distribution nephograms of the magnetic wheel with 2 magnetic tiles adsorbed at the magnet joint

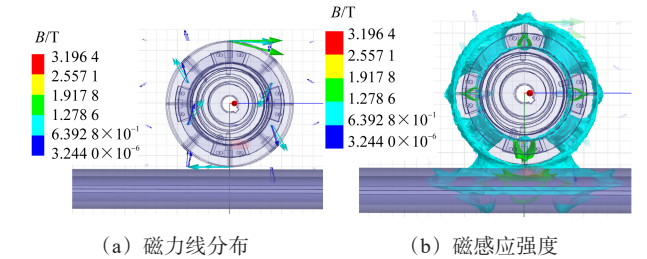


图12 磁瓦拼接处吸附时4块磁瓦磁轮的磁力线分布及磁感应强度云图

云图

Fig. 12 Magnetic field lines and magnetic induction intensity distribution nephograms of the magnetic wheel with 4 magnetic tiles adsorbed at the magnet joint

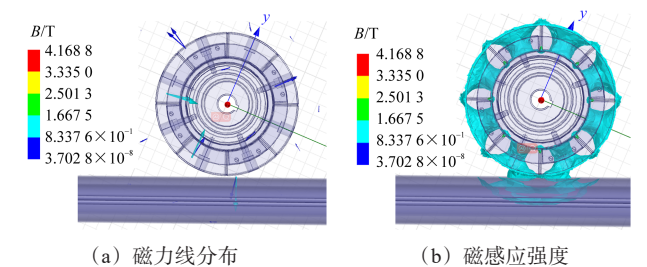


图13 磁瓦拼接处吸附时8块磁瓦磁轮的磁力线分布及磁感应强度云图

Fig. 13 Magnetic field lines and magnetic induction intensity distribution nephograms of the magnetic wheel with 8 magnetic tiles adsorbed at the magnet joint

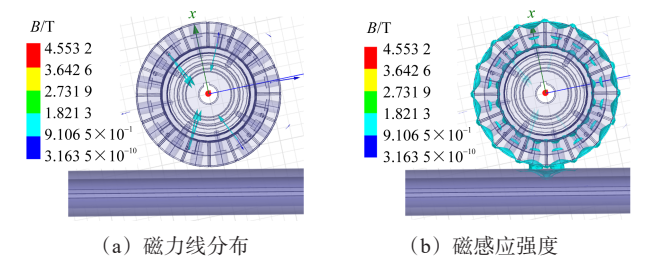


图14 磁瓦拼接处吸附时16块磁瓦磁轮的磁力线分布及磁感应强度云图

Fig. 14 Magnetic field lines and magnetic induction intensity distribution nephograms of the magnetic wheel with 16 magnetic tiles adsorbed at the magnet joint

由表1可知，当磁轮在磁铁拼接处吸附时，4块磁瓦排布的磁轮磁吸力最大，与磁轮磁感应强度云图的分析结果一致。

表1 磁铁拼接处吸附时不同排布方式磁轮的磁吸力

Tab.1 Magnetic attraction forces of magnetic wheels with different arrangement modes when adsorbed at magnet joints

磁轮种类	磁轮磁吸力/N
2块磁瓦排布	823
4块磁瓦排布	1 800
8块磁瓦排布	1 308
16块磁瓦排布	630

2.2 单块磁瓦中间处吸附仿真分析

对单块磁瓦中间处吸附水冷壁管进行距离2 mm相同工况条件下的仿真分析。图15~图18为4种不同排布方式磁轮磁力线分布及磁感应强度云图。

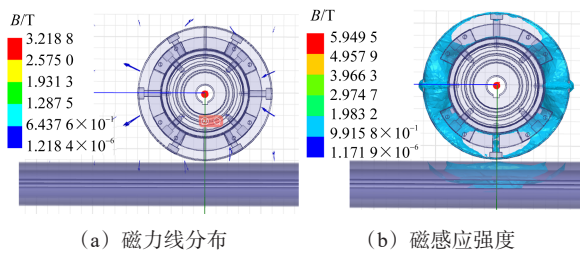


图15 磁瓦中间处吸附时2块磁瓦磁轮的磁力线分布及磁感应强度云图

Fig. 15 Magnetic field lines and magnetic induction intensity distribution nephograms of the magnetic wheel with 2 magnetic tiles adsorbed at the magnet middle

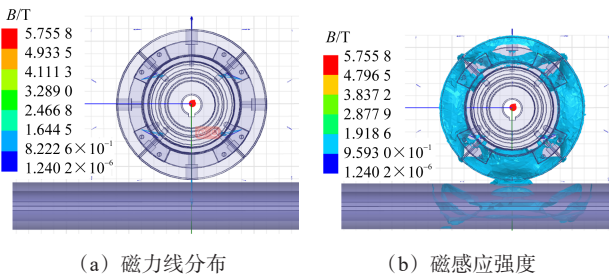


图16 磁瓦中间处吸附时4块磁瓦磁轮的磁力线分布及磁感应强度云图

Fig. 16 Magnetic field lines and magnetic induction intensity distribution nephograms of the magnetic wheel with 4 magnetic tiles adsorbed at the magnet middle

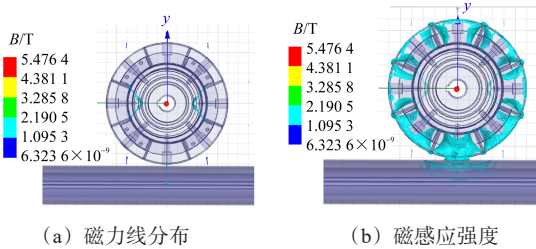


图17 磁瓦中间处吸附时8块磁瓦磁轮的磁力线分布及磁感应强度云图

Fig. 17 Magnetic field lines and magnetic induction intensity distribution nephograms of the magnetic wheel with 8 magnetic tiles adsorbed at the magnet middle

由图15~图18可知, 距水冷壁管2 mm、单块磁瓦中间处吸附时, 4块磁瓦排布磁轮磁感应强度较其他3种排布方式大。磁瓦中间处吸附时4种排布方式磁轮距离水冷壁管2 mm时产生的磁吸力如表2所示。

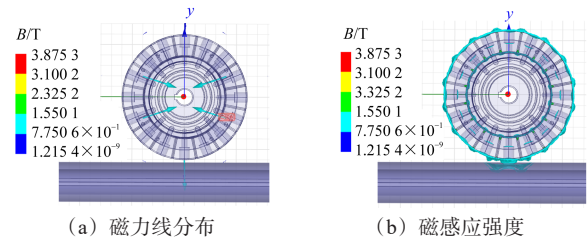


图18 磁瓦中间处吸附时16块磁瓦磁轮的磁力线分布及磁感应强度云图

Fig. 18 Magnetic field lines and magnetic induction intensity distribution nephograms of the magnetic wheel with 16 magnetic tiles adsorbed at the magnet middle

表2 磁轮压3根管且磁瓦中间处吸附时不同排布方式磁轮的磁吸力

Tab.2 Magnetic attraction forces of magnetic wheels with different arrangement modes when pressing against three tubes and adsorbed at the magnet middle

磁轮种类	磁轮磁吸力/N
2块磁瓦排布	783
4块磁瓦排布	1 485
8块磁瓦排布	1 160
16块磁瓦排布	535

由表2可知, 在磁轮单块磁瓦中间处吸附时, 4块磁瓦排布的磁轮磁吸力最大, 与磁轮磁感应强度云图分析结果一致。

2.3 磁轮压2根管单块磁瓦中间处吸附仿真分析

为对比分析磁轮压2根管与压3根管两种工况下的磁场分布及磁吸力, 以磁轮压2根水冷壁管单块磁瓦中间处吸附水冷壁管进行距离2 mm相同工况条件下的仿真分析。图19~图22为4种不同排布方式磁轮磁力线分布及磁感应强度云图。

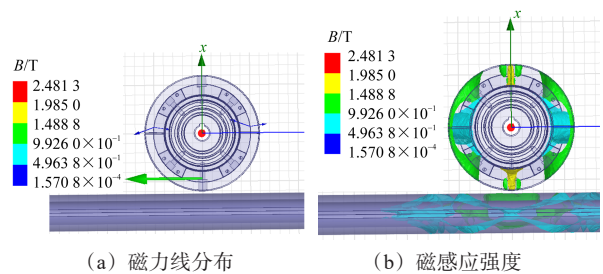


图19 压2根管且磁瓦中间处吸附时2块磁瓦磁轮的磁力线分布及磁感应强度云图

Fig. 19 Magnetic field lines and magnetic induction intensity distribution nephograms of the magnetic wheel with 2 magnetic tiles when pressing against two tubes and adsorbed at the magnet middle

由图19~图22可知, 距水冷壁管2 mm、磁轮压2根水冷壁管单块磁瓦中间处吸附时, 4块磁瓦排布磁轮的磁感应强度较其他3种排布方式大。4种排布方式磁轮距离水冷壁管2 mm时产生的磁吸力如表3所示。

由表3可知, 当磁轮压2根水冷壁管、磁瓦中间处吸附时, 4块磁瓦排布的磁轮磁吸力最大, 与磁轮磁感应强度云图分析结果一致。

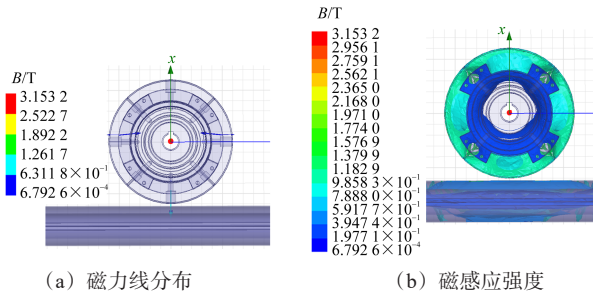


图 20 压 2 根管且磁瓦中间处吸附时 4 块磁瓦磁轮的磁力线分布及磁感应强度云图

Fig. 20 Magnetic field lines and magnetic induction intensity distribution nephograms of the magnetic wheel with 4 magnetic tiles when pressing against two tubes and adsorbed at the magnet middle

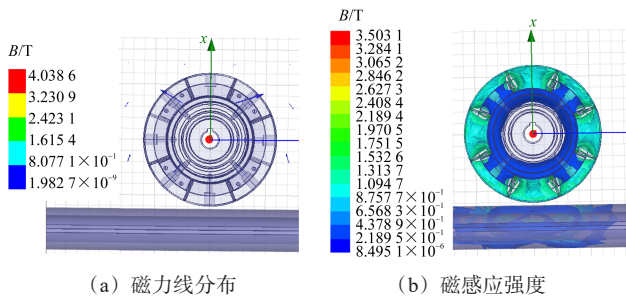


图 21 压 2 根管且磁瓦中间处吸附时 8 块磁瓦磁轮的磁力线分布及磁感应强度云图

Fig. 21 Magnetic field lines and magnetic induction intensity distribution nephograms of the magnetic wheel with 8 magnetic tiles when pressing against two tubes and adsorbed at the magnet middle

对比表 2 与表 3 中数据可知, 磁轮磁瓦中间处吸附、磁轮压 3 根水冷壁管时磁吸力比压 2 根水冷壁管时磁吸力大 10%~20%。

表 3 磁轮压 2 根管且磁瓦中间处吸附时不同排布方式磁轮的磁吸力
Tab. 3 Magnetic attraction forces of magnetic wheels with different arrangement modes when pressing against two tubes and adsorbed at magnet middle and adsorbed at the magnet middle

磁轮种类	磁轮磁吸力/N
2 块磁瓦排布	720
4 块磁瓦排布	1 225
8 块磁瓦排布	964
16 块磁瓦排布	443

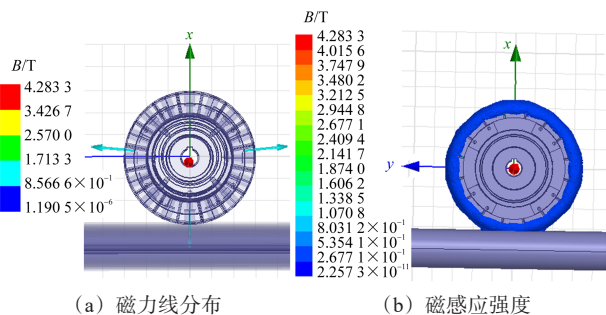


图 22 压 2 根管且磁瓦中间处吸附时 16 块磁瓦磁轮的磁力线分布及磁感应强度云图

Fig. 22 Magnetic field lines and magnetic induction intensity distribution nephograms of the magnetic wheel with 16 magnetic tiles when pressing against two tubes and adsorbed at the magnet middle

3 结论

通过建立 4 种不同排布方式磁瓦磁轮模型, 分析了磁轮磁瓦单块磁铁拼接处及单块磁瓦中间处、磁轮压 3 根水冷壁管距离 2 mm 时的磁场分布情况及磁轮磁吸力; 以单块磁瓦中间处吸附为例, 分析了磁轮压 3 根水冷壁管与磁轮压 2 根水冷壁管工况下的磁场分布情况及磁吸力大小, 得出以下结论:

1) 磁轮单块磁瓦拼接处比单块磁瓦中间处磁感应强度大, 磁轮吸附水冷壁管的磁吸力大 5%~20%; 机器人磁轮设计应以单块磁轮中间处吸附压 2 根管时产生的磁力进行设计计算。

2) 采用 N-S 交替排布的磁轮, 相同体积和质量的磁铁采用 4 块磁瓦排布的磁轮磁吸力较其他几种排布方式大; 磁瓦数量越多, 磁吸力相对越小; 单块磁瓦中间处吸附时, 磁轮压 3 根水冷壁管比磁轮压 2 根壁管的磁吸力大 10%~20%。

3) 本文针对 N-S 交替排布的磁轮磁吸力进行分析, 后续将进一步针对不同结构形式磁铁组合进行分析研究, 为爬壁机器人磁轮结构设计及整机减重优化提供参考。

参 考 文 献

[1] 付宜利,李志海. 爬壁机器人的研究进展[J]. 机械设计,2008, 25(4):1-5.
FU Yili, LI Zhihai. Researching headway of wall-climbing robots [J]. Journal of Machine Design,2008, 25(4): 1-5.

[2] 马涛,李虎,尚飞,等. 爬壁机器人吸附方式机理及其应用[J]. 机械传动,2025,49(3):162-176.
MA Tao, LI Hu, SHANG Fei, et al. Mechanism and application of the adsorption mode for wall-climbing robots[J]. Journal of Mechanical Transmission, 2025, 49(3): 162-176.

[3] 袁夫彩,陆念力,曲秀全. 水下船体清刷机器人磁吸附机构的设计与研究[J]. 中国机械工程,2008,19(4):388-391.
YUAN Fucui, LU Nianli, QU Xiuquan. Design and study on magnetic absorbing machine of underwater robot for cleaning hull[J]. China Mechanical Engineering, 2008, 19(4): 388-391.

[4] 赵智浩,陶友瑞,裴佳星,等. 履带式爬壁机器人磁吸附单元的参数分析与优化[J]. 机械强度,2023,45(3):626-632.
ZHAO Zhihao, TAO Yourui, PEI Jiaying, et al. Parameter analysis and optimization of magnetic adsorption unit for crawler wall-climbing robot[J]. Journal of Mechanical Strength, 2023, 45(3): 626-632.

[5] 塔月月. 轮式爬壁机器人磁吸附性能及磁力控制研究[D]. 大庆:东北石油大学,2012:29-50.
TA Yueyue. Magnetic adsorption capability and adsorptive force

- research of wheeled wall climbing robot [D]. Daqing: Northeast Petroleum University, 2012: 29-50.
- [6] 陈勇,王昌明,包建东. 新型爬壁机器人磁吸附单元优化设计[J]. 兵工学报, 2012, 33(12): 1539-1544.
CHEN Yong, WANG Changming, BAO Jiandong. Optimization of a novel magnetic adsorption unit for wall-climbing robot [J]. Acta Armamentarii, 2012, 33(12): 1539-1544.
- [7] 孙天圣,刘芳华,江来,等. 基于Halbach阵列的爬壁机器人永磁吸附模块优化设计[J]. 机械与电子, 2023, 41(10): 54-59.
SUN Tiansheng, LIU Fanghua, JIANG Lai, et al. Optimal design of permanent magnet adsorption module based on Halbach array for wall-climbing robot [J]. Machinery & Electronics, 2023, 41(10): 54-59.
- [8] 冯玉勇,管殿柱,宋新城,等. 一种中小型船舶检测爬壁机器人吸附能力研究[J]. 青岛大学学报(工程技术版), 2023, 38(4): 71-75.
FENG Yuyong, GUAN Dianzhu, SONG Xincheng, et al. Research on the adsorption capacity of a wall-climbing robot for detecting small and medium-sized ships [J]. Journal of Qingdao University (Engineering & Technology Edition), 2023, 38(4): 71-75.
- [9] 杨怀林,刘春华,陈晓辉,等. 大型球罐壁面除漆机器人设计与实验研究[J]. 机械传动, 2024, 48(1): 151-158.
YANG Huailin, LIU Chunhua, CHEN Xiaohui, et al. Design and experimental study of a large spherical tank wall paint removal robot [J]. Journal of Mechanical Transmission, 2024, 48(1): 151-158.
- [10] 张栋,杨培,黄哲轩,等. 爬壁机器人悬摆式磁吸附机构的设计与优化[J]. 工程设计学报, 2023, 30(3): 334-341.
ZHANG Dong, YANG Pei, HUANG Zhexuan, et al. Design and optimization of pendulous magnetic adsorption mechanism for wall-climbing robots [J]. Chinese Journal of Engineering Design, 2023, 30(3): 334-341.
- [11] 李浩男,侯宇,蒋怡蔚,等. 永磁轮式管外攀爬机器人结构与力学分析[J]. 机械传动, 2023, 47(10): 48-54.
LI Haonan, HOU Yu, JIANG Yiwei, et al. Structural design and mechanical analysis of permanent magnet wheeled climbing robots on an outer wall of pipelines [J]. Journal of Mechanical Transmission, 2023, 47(10): 48-54.

Analysis of magnetic attraction force characteristics of wall-climbing robot magnetic wheels based on Maxwell

ZHANG Wenqiang¹ BIN Guangfu² XU Guangping¹ YANG Wenming¹

(1. Beijing Zhong'an Jitai Technology Co., Ltd., Beijing 100085, China)

(2. Hunan Provincial Key Laboratory of Health Maintenance for Mechanical Equipment, Hunan University of Science and Technology, Xiangtan 411201, China)

Abstract: [Objective] To address the core problems of traditional magnetic tile-type magnetic wheels in the application of boiler wall-climbing robots, such as unclear magnetic field distribution, redundant safety factors of empirical formulas, low magnet utilization rate, and excessive weight, a magnetic tile arrangement scheme was identified with better magnetic attraction in the N-S alternating arrangement under the same volume and mass constraints. The differences in magnetic field distribution and magnetic attraction force magnitude when the magnetic wheel pressed against three versus two boiler water-cooled wall tubes were also clarified. [Methods] Taking a water-cooled wall inspection robot for thermal power plant boilers as an example, four magnetic wheel models with the same external dimensions but different magnet arrangement modes were established. Using Maxwell software, simulation analysis of the magnetic attraction force of these four magnetic wheels with different structures was conducted at a distance of 2 mm from the water-cooled wall tubes. [Results] The results show that the adsorption force of the magnetic wheel on the water-cooled wall tube is 5%-20% greater when adsorbed at the joint of the magnetic tiles than at the middle of the magnetic tiles. When adsorbed at the middle of the magnetic tiles, regardless of whether the magnetic wheel presses against three or two wall tubes, the magnetic wheel with the 4-magnetic-tile arrangement exhibits the maximum attraction. Additionally, the adsorption force when pressing against three water-cooled wall tubes is approximately 10%-20% greater than that when pressing against two tubes.

Key words: Wall-climbing robot; Magnetic wheel; Permanent magnet adsorption; Magnetic attraction force; Wheeled robot

(编辑: 李立)